

# Anomalously large $g$ factor of single atoms adsorbed on a metal substrate

B. Chilian,<sup>1</sup> A. A. Khajetoorians,<sup>1,\*</sup> S. Lounis,<sup>2,†</sup> A. T. Costa,<sup>3</sup> D. L. Mills,<sup>4</sup> J. Wiebe,<sup>1,‡</sup> and R. Wiesendanger<sup>1</sup>

<sup>1</sup>*Institute of Applied Physics, Hamburg University, Jungiusstrasse 11, D-20355 Hamburg, Germany*

<sup>2</sup>*Forschungszentrum Jülich, Peter Grünberg Institut, and Institute for Advanced Simulation, D-52425 Jülich, Germany*

<sup>3</sup>*Instituto de Física, Universidade Federal Fluminense, 24210-340 Niterói, Rio de Janeiro, Brazil*

<sup>4</sup>*Department of Physics and Astronomy, University of California, Irvine, California 92697, USA*

(Received 9 November 2011; revised manuscript received 11 November 2011; published 6 December 2011)

We have performed inelastic scanning tunneling spectroscopy (ISTS) on individual Fe atoms adsorbed on a Ag(111) surface. ISTS reveals a magnetization excitation with a lifetime of about 400 fs, which decreases linearly upon application of a magnetic field. Surprisingly, we find that the  $g$  factor, which characterizes the shift in energy of the excitation in a magnetic field, is  $g = 3.1$  instead of the expected value of 2. This very large  $g$  shift can be understood when considering the complete electronic structure of both the Ag(111) surface state and the Fe atom, as shown by *ab initio* calculations of the magnetic susceptibility.

DOI: [10.1103/PhysRevB.84.212401](https://doi.org/10.1103/PhysRevB.84.212401)

PACS number(s): 75.75.-c, 68.37.Ef, 71.15.-m, 75.40.Gb

Magnetic nanostructures have proved to be of great interest from the perspectives of both fundamental physics and device applications. One finds response characteristics in such systems to be unique to the nano-environment and not realized in bulk magnetic matter. This allows tuning of the magnetic response characteristics of these structures. The smallest magnetic entity is a single moment-bearing atom. Remarkably, scanning tunneling microscope (STM)-based spectroscopy now provides access to the spin dynamics of single atoms in diverse surface environments.<sup>1–11</sup> Previous STM-based studies of isolated Fe atoms on Pt(111)<sup>4,5</sup> and Cu(111)<sup>6</sup> set forth the first data on the strong damping provided by coupling of the spin precession of the moment core to the Stoner excitations of the metallic substrate upon which it is chemisorbed. The data in Ref. 6 also provided the first experimental and *ab initio* verification of a prediction made many years ago: Coulomb interactions alone lead to strong damping of the spin precession of a single moment, when it is both excited and its motion is monitored by a local probe that samples its large-wave-vector response.<sup>12</sup> An excellent account of the data in Ref. 6 was provided by calculations that employ a recently developed formalism.<sup>13–16</sup>

The present Brief Report presents an STM-based study of the excitation spectrum of a single Fe atom on the Ag(111) surface. Utilizing inelastic scanning tunneling spectroscopy (ISTS), we measure the magnetic-field-dependent excitation energy of the Fe atom. The data reveal that the  $g$  factor of the Fe atom assumes the anomalously large value of  $g = 3.1$ . Decades of studies of Fe spin motions in metallic environments by long-wavelength probes such as microwaves or photons (Brillouin scattering) have always shown  $g$  factors within about 5% of the free-electron value of 2. Recent calculations considering the effect of the orbital moment in ISTS have shown considerable *reductions* in  $g$ , but no strong enhancement.<sup>17</sup> We present calculations based on the formalism we have developed,<sup>6,14,16</sup> utilizing the Korringa-Kohn-Rostoker (KKR) Green-function method<sup>18</sup> within time-dependent density-functional theory (TD-DFT),<sup>19,20</sup> that provide an excellent account of the anomalous  $g$  factor found experimentally by considering the many-body Coulomb interactions between the moment-bearing  $d$  electrons and itinerant

electrons in the host. Theoretically, these results are compared to Mn, Cr, and Co atoms in various lattice configurations.

All measurements were obtained in a home-built STM facility with a base temperature of 0.3 K and a magnetic field of up to 12 T perpendicular to the sample surface.<sup>21</sup> The STM tip was made from high-purity Ag wire by cutting and subsequent annealing after transfer into the ultra-high-vacuum facility. The sample was prepared *in situ* by repeated cycles of sputtering with Ar<sup>+</sup> ions and subsequent annealing at a temperature of 550 °C, yielding an atomically flat Ag(111) surface with terraces several hundred nanometers wide. Single Fe atoms were deposited onto the cold sample kept at a temperature of  $T < 6$  K. Differential conductance ( $dI/dV$ ) spectra were obtained by stabilizing the STM tip above the adsorbate with tunneling current  $I_{\text{stab}}$  and bias voltage  $V_{\text{stab}}$  applied to the sample, and by switching off the feedback circuit and ramping the bias voltage  $V$  while recording the  $dI/dV(V)$  signal via lock-in technique with modulation voltage  $V_{\text{mod}} = 50\text{--}100\ \mu\text{V}$  and modulation frequency  $f_{\text{mod}} = 4.1\ \text{kHz}$ .

Figure 1(a) shows high-energy-resolution  $dI/dV$  spectra taken on an isolated Fe atom (inset) with the same microtip for different magnetic field values. In comparison to the spectra taken on a nearby substrate location [Fig. 1(b)], which were always featureless and almost flat, a reduction in the differential conductance signal around the Fermi energy is present. On the positive-bias side, this reduction occurs in the form of a sharp step, whereas on the negative side the decrease of the signal is more gradual. The step on the positive-bias side clearly shifts away from the Fermi energy  $E_F$  (0 V) for increasing magnetic field. To further illustrate the evolution of the two spectroscopic features in a magnetic field, Fig. 1(c) shows an intensity plot of the  $dI/dV$  spectra of a similar dataset as a function of the magnetic field  $B$ , which has been incremented in smaller steps. In the intensity plot, the step at positive bias and a step occurring at a negative bias symmetric with respect to  $E_F$  are visible, and are linearly shifting toward higher absolute bias voltages for increasing magnetic field. We conclude that the two steps are due to a magnetic excitation of the Fe atom by inelastic spin-flip scattering of the tunneling electrons.<sup>6</sup> The corresponding steps in the  $dI/dV$  curves are marked in red in Fig. 1(a). While the excitation step occurs on a

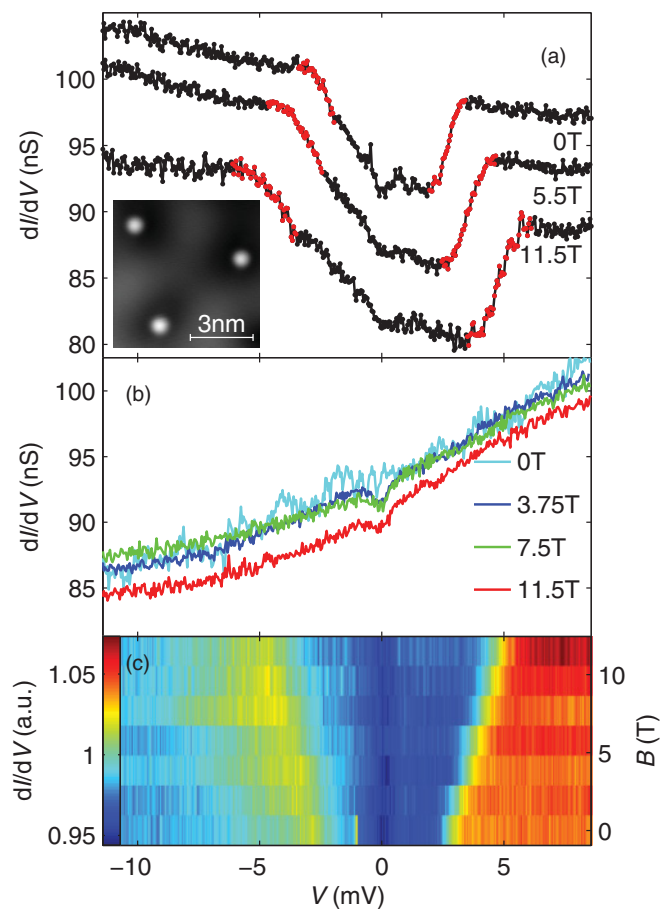


FIG. 1. (Color online) (a) ISTS spectra taken above the Fe adatom for different magnetic fields  $B$  with the same microtip (spectra at 5.5 and 11.5 T are vertically offset by  $-7$  and  $-12$  nS for clarity). On the positive-bias side, the part of the spectrum in the interval  $E_{\text{step}} - w < eV < E_{\text{step}} + w$  is highlighted in red, where  $E_{\text{step}}$  is the fitted step energy and  $w$  is the fitted step width (FWHM; see text). On the negative-bias side, the part of the spectrum on the negative portion of this interval is highlighted. Inset: constant-current image of three Fe atoms on Ag(111) ( $I_{\text{stab}} = 1.3$  nA,  $V_{\text{stab}} = 10$  mV, and gray scale from 0 to 1.35 Å). (b) ISTS spectra taken with the same microtip on the substrate. (c) Color scale representation of a similar dataset taken at smaller increments in the magnetic field. Individual spectra were divided by their mean values for better visualization. ( $I_{\text{stab}} = 1$  nA,  $V_{\text{stab}} = 10$  mV, and  $V_{\text{mod}} = 100$   $\mu$ V.)

rather flat background  $dI/dV$  signal for positive sample bias, it is superimposed on the gradual increase of the  $dI/dV$  signal on the negative sample bias side. The gradual increase does not change with the magnetic field and is observed for all atoms in the filled-states regime, independent of the utilized microtip. Thus, it is probably due to a peak in the local electron density of states (LDOS) above the Fe atom. In all further analysis, only the unmasked step on the positive-bias side was considered.

To extract both the  $g$  factor and the lifetime of the magnetic excitation, ISTS spectra of 17 Fe atoms were analyzed for different magnetic fields, giving a total of 70 data points for each of the following quantities: the step position  $E_{\text{step}}$ , the step width  $w$  (full width at half maximum, FWHM), and the inelastic contribution  $P_{\text{inel}}$  to the total  $dI/dV$  signal for bias voltages greater than the excitation energy. All values have

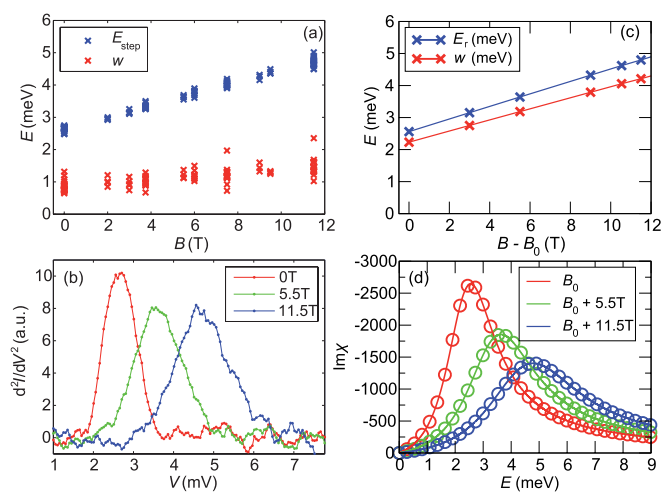


FIG. 2. (Color online) (a) Fitted step energy  $E_{\text{step}}$  and step width  $w$  (FWHM) of the inelastic step on the positive-voltage side of the ISTS spectra taken on 17 different Fe atoms as a function of magnetic field  $B$ . (b) Numerical derivative of the positive-bias part of the spectra used in Fig. 1(a). (c) Calculated magnetic field dependency of the resonance energy  $E_r$  and of the linewidth  $w$ . (d) Examples of computed density of magnetization excitations for an Fe adatom on Ag(111).

been extracted by fitting a Gaussian-broadened step function to the measured spectra in the positive-bias regime. It turns out that  $P_{\text{inel}} = 8.8\% \pm 1.8\%$  [standard deviation (SD)] of the tunneling electrons are inelastically scattered at the Fe atom and induce a spin excitation. Therefore, the process is considerably more efficient than for the case of Fe on Cu(111)<sup>6</sup> or Fe on Pt(111).<sup>4</sup>

The step energy  $E_{\text{step}}$  and width  $w$  are shown in Fig. 2(a) as a function of the magnetic field  $B$ . The step energy shows a zero-field splitting of  $E_{\text{step}}(B = 0 \text{ T}) = 2.7 \pm 0.06$  meV (SD) and then increases linearly with  $B$  with a slope of  $3.13 \pm 0.07 \mu_B$  (SD). The zero-field splitting results from the magnetic anisotropy energy of the Fe moment. The effective  $g$  factor can be extracted from the slope of  $E_{\text{step}}(B)$  by taking into account the selection rules for the excitation of the total angular momentum  $J$  of the adatom-on-substrate system, i.e.,  $\Delta m_J = 0$  or  $\pm 1$ ,<sup>17</sup> resulting in  $g = 3.13 \pm 0.07$ . Finally, as exemplified by the derivative of the spectra of Fig. 1(a) with respect to the voltage shown in Fig. 2(b), there is a significant linewidth broadening of the excitation as the magnetic field is increased. This linewidth increases with a rate of  $\approx 1.1 \mu_B$  [Fig. 1(a)].

As we have shown for the case of Fe adatoms on Cu(111),<sup>6</sup> the linear increase of the linewidth as a function of the excitation energy can be explained by the decay of the excitation into Stoner modes of the itinerant conduction electrons of the substrate.<sup>6,13,14,16</sup> Due to the hexagonal symmetry of the substrate, the measured magnetic anisotropy energy for Ag(111) most probably favors a uniaxial out-of-plane orientation of the Fe moment, as predicted with our simulations using KKR, which reveal a perpendicular magnetic anisotropy of 5.6 meV. Moreover, the experimental value is almost a factor of 3 larger than for Cu(111).<sup>6</sup> Also, the lifetime of the excitation, which is derived from the linewidth at  $B = 0$  T to be  $\tau = \hbar/(2\Delta E) \approx 400$  fs, is about twice as large as for

Cu(111) and decreases with a rate that is two times smaller. Remarkably, the  $g$  factor for the case of Ag(111) is 50% larger than for Cu(111).

In order to elucidate the  $g$  factor enhancement, first-principles calculations have been carried out to evaluate the energy-dependent local transverse spin susceptibility  $\chi(E)$ , whose imaginary part  $\text{Im}(\chi)$  describes the density of states of possible magnetic excitations. The formal expression for the dynamic susceptibility can be written as

$$\chi = \chi_0 / (1 - U\chi_0), \quad (1)$$

connecting the Kohn-Sham susceptibility  $\chi_0$  (which describes Stoner excitations) to the exchange and correlation kernel  $U$ . To mimic spin-orbit coupling, which is not incorporated into our KKR-based formalism, an appropriate external magnetic field  $B_0$  was applied. This approach produced results in excellent accord with the empirical tight-binding description of magnetic excitations of the Fe adatom on Cu(111), where spin-orbit coupling was incorporated.<sup>6</sup>

In Fig. 2(c) we plot the magnetic-field dependence of the theoretical resonance energy  $E_r$  and linewidth  $w$ , which can be directly compared to Fig. 2(a). We find a  $g$  factor of 3.34, which is in a striking agreement with the measured value. The theoretical linewidth ( $B = 0$ ) is about twice the corresponding experimental value and broadens more heavily ( $\approx 2.9\mu_B$ ) than the average measured linewidth ( $\approx 1.1\mu_B$ ). Interestingly, our calculations identify the Fe-adatom  $g$ -factor enhancement as a rare case, since Cr, Mn, and Co adatoms are characterized by typical  $g$  values of 2.1, 1.9, and 1.84 (not shown).

The Ag(111) surface is peculiar since its surface-state onset is located much closer to  $E_F$  compared to Cu(111) and Au(111).<sup>22</sup> Our calculations indicate an onset value of  $-50$  meV [Figs. 3(a) and 3(b)]. Moreover, it is well established that an adatom induces a bound state that is split off from the bottom of the surface-state band if the adatom potential is attractive.<sup>23–26</sup> These effects could principally affect the  $g$  factor. As on the Cu(111) surface, Fe [Fig. 3(c)], as well as Cr, Mn, and Co adatoms (not shown) exhibit a spin-polarized split-off state on the Ag(111) surface. If this bound state is responsible for the large  $g$  shift, it should consequently also induce a large  $g$  shift for Cr, Mn, and Co adatoms. However, this is not seen computationally. Furthermore, these impurities were considered as “inatoms,” i.e., substitutional impurities in the surface layer, and bulk atoms, where no bound-state is present as predicted for the Cu(111) surface.<sup>25</sup> Among all additional impurities investigated, only the Mn inatom exhibits a large  $g$  factor of 2.9, illustrating that the bound state is not necessarily responsible for enhancing the  $g$  factor.

Finally, to investigate the influence of the surface state, we shifted its location by reducing the thickness of the simulated slab from 24 to 5 monolayers. This artificial consideration modifies the surface state, since the two surface states at both ends strongly interact, thereby splitting into bonding and antibonding states. These are then located very far from  $E_F$ . This electronic modification diminishes the  $g$  factor of the Fe adatom to  $g \approx 2$ . This indicates that the electronic properties of the surface state play an important role in the observed  $g$  shift.

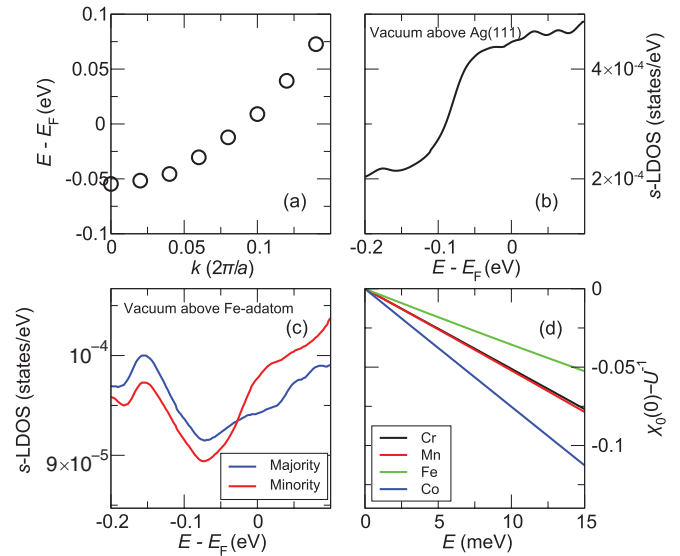


FIG. 3. (Color online) (a) Calculated band structure showing the surface state of Ag(111) centered around the  $\Gamma$  point, where  $a$  is the lattice parameter of Ag. (b) Corresponding calculated steplike  $s$ -LDOS in the vacuum evaluated at 4.7 Å above the surface. (c) If an Fe atom is put on top of the surface, a bound state is created that is spin split. (d) Linear behavior of the real part of the Kohn-Sham susceptibility for different adatoms on Ag(111). The Fe adatom is characterized by the smallest slope reproducing its large  $g$  shift.

While there is not a simple picture of how the interplay of the surface-state electronic structure combined with that of the Fe atoms produces the observed  $g$  shift, a specific trend can be seen in the low-energy properties of the susceptibility, which may explain the observed  $g$  shift. Since we probe energies far below the electronic scale, we can expand  $\chi_0(E)$  in powers of the energy  $E$  if desired. For small energies, it can be shown that the real part  $\text{Re}(\chi_0)$  and the imaginary part  $\text{Im}(\chi_0)$  of the Kohn-Sham susceptibility are linear functions of  $E$ , i.e.,  $\text{Re}(\chi_0(E)) = \chi_0(0) + \alpha E$  and  $\text{Im}(\chi_0(E)) = \beta E$ .  $\chi_0(0)$  is the static susceptibility and  $\text{Im}(\chi_0)$  describes the density of Stoner modes, while  $\alpha$  and  $\beta$  are the slopes defining the linear energy dependence. Analytically,  $\beta$  is given by the product between the spin-dependent adatom density of states at  $E_F$  [ $-\pi n_{\downarrow}(E_F)n_{\uparrow}(E_F)$ ], while  $\alpha$  is more complex but can be expressed in terms of single-particle Green functions evaluated at  $E_F$ .

In Fig. 3(d),  $\text{Re}(\chi_0)$  at  $B = 0$  is plotted against energy for Cr, Mn, Fe, and Co adatoms on Ag(111), and indeed the trend is linear and is not modified with an applied field. Interestingly,  $\alpha$  is smallest for the Fe adatom, which strongly contributes to the large  $g$  shift. In fact, by plugging the linear behavior of  $\chi_0$  into Eq. (1) and evaluating  $\text{Im}(\chi)$  we obtain an equation similar to what is given in Refs. 12 and 13:

$$\text{Im}(\chi) = \frac{\beta E}{\{1 - U[\chi_0(0) + \alpha E]\}^2 + (U\beta E)^2}, \quad (2)$$

where the resonance energy  $E_r = |\frac{1}{U} - \chi_0(0)| / \sqrt{\alpha^2 + \beta^2}$ . If no external magnetic field is applied along the  $z$  direction,  $\chi_0(0) = 1/U$ <sup>14,16</sup> and consequently  $E_r = 0$ . This is a key result: The position of the resonance, and thus the  $g$  shift,

depends equally on the slope of  $\text{Re}(\chi_0)$ , the slope of  $\text{Im}(\chi_0)$ , and the change of  $\chi_0$  at zero energy induced by the magnetic field. Thus the right combination of these properties must be satisfied in order to observe a large  $g$  shift as for the Fe adatom.

This new data, combined with that in Ref. 6 where the  $g$  factor in both the data and theory is close to 2, shows that  $3d$  transition-metal moments on metal surfaces can display a wide range of response characteristics not realized with long-wavelength probes of bulk materials. In contrast to the spin-orbit-induced  $g$  shift that is operative in long wavelength probes, the large shift present in both the data and the calculations presented here has its origin only in the Coulomb interaction between the electrons, a feature unique to the

response of the moment when probed with atomic-scale spatial resolution.<sup>12</sup> This Brief Report presents data in which this large Coulomb-induced  $g$  shift, predicted over forty years ago,<sup>12</sup> has been experimentally observed and confirmed by *ab initio* calculations of local spin dynamics.

We would like to thank W. Wulfhekel and P. Gambardella for fruitful discussions. We acknowledge funding from Grants No. SFB668-A1 and No. GrK1286 of the DFG, from ERC Advanced Grant “FUORE,” and from the Cluster of Excellence “Nanospintronics.” The research of D.L.M. and A.T.C. was supported by the US Department of Energy via Grant No. DE-FG03-84ER-45083. S.L. acknowledges the support of HGF-YIG Programme No. VH-NG-717.

\*akhajeto@physnet.uni-hamburg.de

†s.lounis@fz-juelich.de

‡Corresponding author: jwiebe@physnet.uni-hamburg.de

<sup>1</sup>A. J. Heinrich, J. A. Gupta, C. P. Lutz, and D. M. Eigler, *Science* **306**, 466 (2004).

<sup>2</sup>C. F. Hirjibehedin, C.-Y. Lin, A. F. Otte, M. Ternes, C. P. Lutz, B. A. Jones, and A. J. Heinrich, *Science* **317**, 1199 (2007).

<sup>3</sup>A. A. Khajetoorians, B. Chilian, J. Wiebe, S. Schuwalow, F. Lechermann, and R. Wiesendanger, *Nature (London)* **467**, 1084 (2010).

<sup>4</sup>T. Balashov, T. Schuh, A. F. Takács, A. Ernst, S. Ostanin, J. Henk, I. Mertig, P. Bruno, T. Miyamachi, S. Suga, W. Wulfhekel, *Phys. Rev. Lett.* **102**, 257203 (2009).

<sup>5</sup>T. Schuh, T. Balashov, T. Miyamachi, A. F. Takacs, S. Suga, and W. Wulfhekel, *J. Appl. Phys.* **107**, 09E156 (2010).

<sup>6</sup>A. A. Khajetoorians, S. Lounis, B. Chilian, A. T. Costa, L. Zhou, D. L. Mills, J. Wiebe, and R. Wiesendanger, *Phys. Rev. Lett.* **106**, 037205 (2011).

<sup>7</sup>J. Fernández-Rossier, *Phys. Rev. Lett.* **102**, 256802 (2009).

<sup>8</sup>N. Lorente and J.-P. Gauyacq, *Phys. Rev. Lett.* **103**, 176601 (2009).

<sup>9</sup>J. Fransson, *Nano Lett.* **9**, 2414 (2009).

<sup>10</sup>S. Loth, C. Lutz, and A. Heinrich, *New J. Phys.* **12**, 125021 (2010).

<sup>11</sup>F. Delgado and J. Fernández-Rossier, *Phys. Rev. B* **84**, 045439 (2011).

<sup>12</sup>D. L. Mills and P. Lederer, *Phys. Rev.* **160**, 590 (1967).

<sup>13</sup>R. B. Muniz and D. L. Mills, *Phys. Rev. B* **68**, 224414 (2003).

<sup>14</sup>S. Lounis, A. T. Costa, R. B. Muniz, and D. L. Mills, *Phys. Rev. Lett.* **105**, 187205 (2010).

<sup>15</sup>A. T. Costa, R. B. Muniz, S. Lounis, A. B. Klautau, and D. L. Mills, *Phys. Rev. B* **82**, 014428 (2010).

<sup>16</sup>S. Lounis, A. T. Costa, R. B. Muniz, and D. L. Mills, *Phys. Rev. B* **83**, 035109 (2011).

<sup>17</sup>T. Schuh, T. Balashov, T. Miyamachi, S.-Y. Wu, C.-C. Kuo, A. Ernst, J. Henk, and W. Wulfhekel, *Phys. Rev. B* **84**, 104401 (2011).

<sup>18</sup>N. Papanikolaou, R. Zeller, and P. H. Dederichs, *J. Phys. Condens. Matter* **14**, 2799 (2002).

<sup>19</sup>E. Runge and E. K. U. Gross, *Phys. Rev. Lett.* **52**, 997 (1984).

<sup>20</sup>E. K. U. Gross and W. Kohn, *Phys. Rev. Lett.* **55**, 2850 (1985).

<sup>21</sup>J. Wiebe, A. Wachowiak, F. Meier, D. Haude, T. Foster, M. Morgenstern, and R. Wiesendanger, *Rev. Sci. Instrum.* **75**, 4871 (2004).

<sup>22</sup>F. Reinert, G. Nicolay, S. Schmidt, D. Ehm, and S. Hüfner, *Phys. Rev. B* **63**, 115415 (2001).

<sup>23</sup>F. E. Olsson, M. Persson, A. G. Borisov, J.-P. Gauyacq, J. Lagoute, and S. Fölsch, *Phys. Rev. Lett.* **93**, 206803 (2004).

<sup>24</sup>L. Limot, E. Pehlke, J. Kröger, and R. Berndt, *Phys. Rev. Lett.* **94**, 036805 (2005).

<sup>25</sup>S. Lounis, P. Mavropoulos, P. H. Dederichs, and S. Blügel, *Phys. Rev. B* **73**, 195421 (2006).

<sup>26</sup>B. Lazarovits, L. Szunyogh, and P. Weinberger, *Phys. Rev. B* **73**, 045430 (2006).